Optogenetic and transcriptomic interrogation of enhanced muscle function in the paralyzed mouse whisker pad

Thomas J. Vajtay [1 #], Akhil Bandi [1 #], Aman Upadhyay [1], Mavis. R. Swerdel [1], Ronald P. Hart [1], Christian R. Lee [1], David J. Margolis [1 *]

[1] Department of Cell Biology and Neuroscience, Rutgers, The State University of New Jersey, Piscataway NJ, 08854, USA
[#] Co-first author contribution
* Correspondence: david.margolis@rutgers.edu; +1 848-445-9533

Abstract

The functional state of denervated muscle is a critical factor in the ability to restore movement after injury- or disease-related paralysis. Here we used peripheral optogenetic stimulation and transcriptome profiling in the mouse whisker system to investigate the time course of changes in neuromuscular function following complete unilateral facial nerve transection. While most skeletal muscles rapidly lose functionality after lower motor neuron denervation, optogenetic muscle stimulation of the paralyzed whisker pad revealed sustained increases in the sensitivity, velocity, and amplitude of whisker movements, and reduced fatigability, starting 48 h after denervation. RNA-seq analysis showed distinct regulation of multiple gene families in denervated whisker pad muscles compared to the atrophy-prone soleus, including prominent changes in ion channels and contractile fibers. Together, our results define the unique functional and transcriptomic landscape of denervated facial muscles, and have general implications for restoring movement after neuromuscular injury or disease.

Keywords: Denervation, mystacial vibrissae, motor control, plasticity, sensorimotor integration, movement disorders, paralysis, optogenetics, ChR2, RNA-seq

New & Noteworthy: Optogenetic activation of muscle can be used to non-invasively induce movements and probe muscle function. We used this technique in mice to investigate changes in whisker movements following facial nerve transection. We found unexpectedly enhanced functional properties of whisker pad muscle following denervation, accompanied by unique transcriptomic changes. Our findings highlight the utility of the mouse whisker pad for investigating the restoration of movement after paralysis.

INTRODUCTION

The functional state of denervated muscle is critical for the restoration of movement after paralysis caused by chronic injury or disease. Functional changes in muscle are well known after lower motor neuron denervation for many types of muscle (Thesleff 1974, Wu et al 2014), with loss of function, atrophy and reduced capacity for movement being the most common. Gain-of-function changes can also occur in parallel, including increased excitability and hypersensitivity to the neurotransmitter acetylcholine (Jones & Vrbova 1974, Lomo & Rosenthal 1972, Sellin & Thesleff 1980). However, gain-of-function changes do not counteract the atrophy and loss of function in most muscles, which presents major problems for generation of contractile force and the ability of muscle to respond to restorative interventions. Furthermore, available clinical strategies to stimulate neuromuscular function generally target a partially intact nerve instead of direct stimulation of the muscle because it is difficult to produce well-controlled, graded movements using electrical stimulation of muscle (Doucet et al 2012, Griffin & Kim 2011, Ho et al 2014, Peckham & Knutson 2005). Non-invasive, direct stimulation of paralyzed muscle that produces naturalistic movements is highly desirable but has not been achieved using traditional methods.

Our previous work established a method for non-invasive control of whisker movements in mice using transdermal photostimulation of the optogenetic actuator channelrhodopsin-2 (ChR2) expressed in whisker pad muscles (Park et al 2016). Spot illumination of the rostral whisker pad with blue light in Emx1-ChR2 mice, as used in the previous and current work, evokes whisker protractions by activating extrinsic protractor muscles pars media superior and pars media inferior of *M. nasolabialis profundus* and also intrinsic follicular muscles (Haidarliu et al 2015, Haidarliu et al 2010, Park et al 2016), collectively referred to here as “whisker pad muscles”. In the present study, we used ChAT-ChR2 and Emx1-ChR2 mice to evoke whisker movements via stimulation of the facial motor nerve (cranial nerve VII) or the whisker pad muscles, respectively. This allowed us to investigate the functional changes that occur in nerve and muscle after the paralysis of whisker movements caused by facial nerve transection.

One recent study used optogenetic muscle stimulation in the hindlimb triceps surae after sciatic nerve lesion to demonstrate dramatic atrophy and loss of function (Magown et al 2015), consistent with classic studies in this system (Nelson 1969), that could be attenuated by daily optogenetic activation. We considered it possible that whisker pad muscles undergo distinct denervation-induced changes compared to other muscle types, in part because whisker pad

72 muscles are composed of distinctive fiber type (Haidarliu et al 2010, Jin et al 2004). While the
73 rodent whisker system has been used for studies related to recovery of function and
74 reinnervation (Hadlock et al 2005, Heaton et al 2014), the functional state of denervated whisker
75 pad muscles and their capacity to support evoked movements has remained unclear, in part
76 because non-invasive methods to probe muscle function have only recently been established.
77
78 We longitudinally tracked whisker movements evoked by optogenetic nerve or muscle
79 stimulation up to 10 d after facial nerve transection. While nerve-evoked responses degraded by
80 1 d, muscle-evoked whisker protractions showed dramatic increases in sensitivity, amplitude,
81 velocity, and reduced fatigability. Furthermore, RNA-seq analysis of denervated muscle at days
82 1, 3 and 7 revealed transcriptome-level changes in ion channels and contractile fibers (among
83 others), with many striking differences compared to published data from the atrophy-prone
84 soleus muscle. Our results could lead to development of treatment strategies for restoring
85 function in various types of paralyzed muscle.
86
87

88 **METHODS**

89 **Subjects and surgical preparation**

90 Procedures were approved by Rutgers University Institutional Animal Care and Use Committee.
91 Mice were purchased from Jackson Labs (Bar Harbor, ME) and bred in house. ChR2
92 expression was driven in nerve crossing Ai32 Cre-dependent ChR2 reporter mice (B6;129S-
93 Gt(ROSA)26Sortm32(CAG-COP4*H134R/EYFP)Hze/J; Jax 012569) with ChAT-Cre mice
94 (B6;129S6-Chattm2(cre)Lowl/J; Jax 006410) to produce “Chat-ChR2” mice. Chat-ChR2 mice
95 express ChR2 in cholinergic neurons, including motoneurons (Rossi et al 2011). Ai32 mice were
96 crossed with Emx1-Cre mice (B6.129S2-Emx1tm1(cre)Krj/J; Jax 005628) to produce “Emx1-
97 ChR2” mice (Madisen et al 2012) that express ChR2 in whisker pad muscles (Park et al 2016).
98 Additional groups of mice were used for pharmacological effects on fasciculations (n=5) and
99 RNA-seq (n=9) experiments (below). Emx1-ChR2 mice on the day of lesion were postnatal day
100 (P) 52 or P55. Additional Emx1-ChR2 mice used for ChR2 expression measures were P75 on
101 the day of lesion. ChAT-ChR2 mice were P276 on the day of lesion. Mice were median age
102 P224 (range P159-224) for RNA-seq experiments. Both male and female mice were used, with
103 weights between 19 and 38 g.

For optogenetic stimulation, adult mice were implanted with a head post affixed to the skull with dental cement in a surgical procedure under isoflurane anesthesia, as described (Lee & Margolis 2016, Park et al 2016), and allowed to recovery for at least 5 d. After baseline measurements were taken, facial nerve transection was performed following (Olmstead et al 2015) in a second surgery. Briefly, mice were anesthetized with isoflurane (4% induction, 2% maintenance) and depilatory cream was applied to an approximately 1x1 cm area caudal to the whisker pad between the eye and jaw. A dorsoventral skin incision was made using spring scissors, and the buccal and superior marginal branches of the facial nerve exposed before transection with spring scissors. The wound margin was closed using cyanoacrylate glue and mice allowed to recover in the home cage. Unilateral whisker movement paralysis was visually verified.

Stimuli and video recording

Light stimuli and recording methods followed our previous work (Park et al 2016). Briefly, a blue 460 nm high-power LED (Prizmatix) was coupled to a 200 μm diameter optical fiber (Thorlabs), producing a 2-3 mm spot of light on the face. Video of whiskers was recorded at 500 frames/s with a high-speed CMOS camera (PhotonFocus, DR1) under infrared illumination (Advanced Illumination). 8 mW stimuli of varying duration were triggered using TTL pulses sent by Arduino microcontroller to the LED current controller. Movies of 3 s duration were recorded for each trial with a 5 s or 15 s inter-trial interval for Emx1-ChR2 and ChAT-ChR2 mice respectively. Sequential trials increased in stimulus duration up to 1000 ms, at which point the sequence was repeated. There were 8 replicates of each stimulus duration for each mouse. To identify the position of the nerve in ChAT-ChR2 mice, the buccal branch of the facial nerve (cranial nerve VII) was targeted with the light spot at a position between the stylomastoid foramen, ventral to the ear canal and caudal to the whisker pad. Different illumination positions in this region were tested for each subject to optimize the evoked whisker protraction. To test effects on fasciculations, dantrolene (1 mM) was applied subcutaneously to the lesioned (right-side) whisker pad. The placement of LED for muscle stimulation in Emx1-ChR2 mice followed Park et al (2016) to target the rostral protraction or caudal retraction area.

Whisker tracking and measurements

Frame-by-frame whisker angle was extracted using routines in Matlab and Python (Clack et al 2012). Video artifacts were corrected using ImageJ if the whiskers were mislabeled. Time series

136 data from individual whiskers were further analyzed in Matlab, including maximum amplitude,
137 velocity (peak of first derivative after Savitzky-Golay smoothing of single trials) and time-to-
138 peak. Persistence index, a measure of fatigability, was calculated for 1000 ms stimuli as the
139 ratio of response amplitude at 1000 ms to peak amplitude. Spectral analysis of fasciculations
140 was performed using the fast Fourier transform (FFT) function within Matlab. Data from trials
141 were averaged within and then between mice. Statistics were calculated using linear mixed
142 models using the lme4 R package. Post hoc testing was done with paired contrasts via the
143 multcomp R package and p values were adjusted for multiplicity with the Holm-Bonferroni
144 method.

145 **RNA-seq**

146 A separate group (n=9 mice) was used for tissue extraction for RNA-seq. Nerve transection was
147 performed as above, with the addition of a sham control on the opposite whisker pad, where the
148 skin was opened and re-closed but the nerve was not lesioned. At 1, 3, and 7 d post-lesion,
149 mice were anesthetized with isoflurane (4% induction) and the fur trimmed to the level of the
150 skin, then killed by cervical dislocation. Skin and muscle tissue was harvested bilaterally from
151 lesioned and intact rostral whisker pads using a 3 mm circular biopsy punch at the site of the
152 rostral protraction area used for optogenetic stimulation. Biopsied tissue was flash-frozen in
153 liquid nitrogen and ground with ceramic mortar and pestle prior to Trizol extraction. Sequencing
154 libraries were prepared with the Illumina TruSeq RNA Sample Preparation Kit v2 and then RNA-
155 seq was performed with the Illumina NextSeq 500. qPCR was used to verify selected genes.
156 Comparisons were made between lesioned and sham-control sides as well as a soleus dataset
157 from GEO: GSE58669 (Macpherson et al 2015) after replicating the latter analysis in our
158 framework to determine significant genes. RNA-seq data have been uploaded to NIH GEO with
159 accession number GSE121590.
160
161 Illumina bcl2fastq2-v2.17.1.14 software was used for basecalling. Sequences were de-
162 duplicated with ParDRe version 2.1.5-PC170509. Adapter sequences were trimmed and QC
163 performed with Fastp version 0.12.2. De-duplicated, trimmed sequences were aligned with
164 ENSEMBL GRCm38 cDNA transcripts using Kallisto version 0.43.1 with 100 bootstrap
165 simulations (-b 100). Kallisto transcript counts were loaded into Sleuth version 0.30.0. The linear
166 model for likelihood ratio test (LRT) was ~ days:days + injury. A Wald test (WT) was evaluated
167 for each day by separately loading in respective data and comparing sides. The significant WT
168 transcripts were then filtered with the differentially expressed transcripts from the LRT and

limited to only those transcripts with at least a 2 FC. Enriched GO terms were determined by creating a list of the gene ID's of all 2 FC transcripts calculated from the WT, sorted by FC, and then analyzed with clusterProfiler for both cellular component and biological process enriched GO terms. Enriched GO terms for whisker 3 d were: GO:0014704; GO:0031674; GO:0043292; GO:1902495; GO:0005892; GO:0034702; GO:0030018; GO:0042641; GO:0000151; GO:0001518. Enriched GO terms for soleus 3 d were GO:1902495; GO:0005901; GO:0034702; GO:0008076; GO:0014704; GO:0042383; GO:0043292; GO:0043235; GO:0016528.

The transcripts from significant GO terms were then compared between whisker and soleus data in heatmaps. Normalized transcripts per million were used to calculate a z-score of the injured expression levels for each day separately and then only those transcripts that were differentially expressed in at least one of the data sets were isolated. To further isolate transcripts of interest, we then limited the selection to only those transcripts that had polar expression between whisker and soleus 3 d.

Quantitative real-time PCR (qPCR)

qPCR was used to validate RNA-seq results and to test for changes in ChR2 expression Supplemental Fig. 4 (goo.gl/sb75Qd). Total cellular RNA was reverse transcribed into cDNA, then assayed by qPCR using SYBR Green PCR Master Mix (Life Technologies) following the manufacturer's recommendations. Primers were designed to be specific using Primer-BLAST. Beta-Actin was used to normalize expression levels to obtain relative quantity (RQ) values. Forward and reverse primers are listed in Supplemental Fig. 4 (goo.gl/sb75Qd).

Data availability

Data and code to recreate figures and statistics are available at https://github.com/margolislab/Vajtay_Bandi_2018. Source data are available upon reasonable request. RNA-seq dataset is available at https://www.ncbi.nlm.nih.gov/geo/query/acc.cgi?acc=GSE121590.

RESULTS

We aimed to determine the functional and transcriptomic state of denervated (paralyzed) whisker pad muscle. We used longitudinal optogenetic methods to investigate the time course

203 of whisker movements evoked by nerve or muscle stimulation up to 10 d after facial nerve
204 transection, and in parallel, generated RNA-seq datasets on 1, 3 and 7 d.
205
206 **Rapid loss of nerve-evoked movements.** We first performed optogenetic stimulation of the
207 facial nerve in ChAT-ChR2 mice to determine the time course of functional denervation after
208 nerve transection (**Fig. 1A**). Prior to nerve transection, transdermal illumination of the buccal
209 branch caudal to the whisker pad evoked brief, high-velocity whisker protractions (peak
210 amplitude, 8.77 ± 1.55°; peak velocity, 940 ± 161°/s; time to peak, 16.2 ± 0.93 ms; half width,
211 13.8 ± 1.16 ms SEM; n=6 mice). After facial nerve transection caudal to the illumination site,
212 whisker movements could still be evoked at 0.5 and 6 h post-lesion, but were abolished by 24 h
213 (**Fig. 1B**). Responses to brief (5 ms) or prolonged (1000 ms) 8 mW illumination were similar in
214 both amplitude and velocity, suggesting that the facial nerve responds to optogenetic stimuli in
215 an all-or-none fashion to suprathreshold stimuli. Analysis of group data from n=6 mice indicated
216 that peak amplitude and peak velocity decreased in parallel over 24 h (**Fig. 1C, left, middle**). At
217 the 6 h time point, peak amplitude decreased compared to baseline in 5/6 mice, and was fully
218 abolished in 6/6 mice by 24 h (ANOVA of peak amplitude and peak velocity over days, F=31.16
219 and 37.88, p=0.0008 and 0.0005). The time-to-peak and half-width of the responses remained
220 similar at the 6 h time point until responses were abolished at 24 h (**Fig. 1C, right**) (ANOVA of
221 time-to-peak and half-width 1000 ms light response over days, F=58.19 and 22.07, p=1.7e-8
222 and 1.5e-6). During the course of nerve degradation (at 6 h), response duration families for
223 peak amplitude and peak velocity showed similar overall shape and stimulus threshold (**Fig. 1D,**
224 **left, middle**). Time-to-peak and half-width measures were constant when probed with stimuli of
225 varying duration (**Fig. 1D, right**), indicative of stereotyped all-or-none nature of whisker
226 movements evoked by suprathreshold optogenetic nerve stimulation. Together, these results
227 indicate that the distal cut end of the facial nerve remains viable for at least 6 h, retaining its
228 ability to evoke whisker movements in response to optogenetic stimulation, but fully degrades
229 by the 24 h time point. Thus, whisker pad muscles are functionally denervated by 24 h after
230 facial nerve transection.
231
232 **Spontaneous fasciculations.** We observed spontaneous small-amplitude whisker twitches on
233 the lesioned side after nerve transection (2.45 ± 0.54° peak-to-peak amplitude, n=9 mice),
234 reflecting fasciculations (or fibrillations) of the denervated muscle fibers (Heaton & Kobler 2005,
235 Salafsky et al 1968, Thesleff & Ward 1975, Wu et al 2014) (**Fig. 2A**). Fasciculation strength, as
236 indicated by spectral analysis, increased in 7/9 mice at 2 d and 9/9 mice at 3 d post-lesion, and

237 persisted through 10 d (**Fig. 2B**) (ANOVA of average power of fasciculations at 5-8 Hz over
238 days, F=36.3, p<2.2e-16). In a separate group of mice, we tested the effects of the ryanodine
239 receptor 1 (RyR1) antagonist dantrolene (1 mM) by subcutaneous whisker pad administration
240 before and 7 d after nerve transection, and found that dantrolene abolished fasciculations (**Fig.**
241 **2C**) (ANOVA of average power of fasciculations at 5-8 Hz of DMSO, Dantrolene, and untreated
242 mice before and 7 d after lesion, F=7.98, p=0.002; Paired contrasts of 7 d Dantrolene versus 7 d
243 DMSO vehicle, t=2.95, p=0.04; n=5 mice), indicating a postsynaptic muscle origin. These
244 results suggest that denervated whisker pad muscles undergo changes in intrinsic excitation-
245 contraction coupling or excitability, raising the question of their capacity to sustain evoked
246 movements.
247
248 **Denervation-induced enhancement of optogenetic muscle-evoked whisker movements.**
249 To determine functional properties of denervated whisker pad muscle, we used direct
250 optogenetic muscle stimulation in Emx1-ChR2 mice following facial nerve transection (**Fig. 3A**).
251 Emx1-ChR2 mice express ChR2 in whisker pad muscles (Park et al 2016) in addition to the
252 well-known expression in excitatory cortical neurons (Madisen et al 2012). We performed
253 longitudinal measurements of the same subjects, similar to the nerve experiments in figure 1,
254 but over a longer time course up to 10 d. Transdermal illumination of the rostral protraction area
255 (Park et al 2016) of the whisker pad under baseline conditions evoked robust whisker
256 protractions (peak amplitude, 13.9 ± 1.6°; peak velocity, 414.8 ± 75.8°/s; 97.85 ± 14.26 ms time
257 to peak; 368.17 ± 86.80 ms half width, n=9 mice) that adapted (or fatigued) during prolonged
258 illumination. After facial nerve transection, peak amplitude and peak velocity of evoked
259 movements began to increase on subsequent days, as shown for an example subject (**Fig. 3B**).
260 Analysis of group data (n=9 mice) showed prominent increases in peak amplitude, peak
261 velocity, and persistence index (a measure of reduced fatigability, see below) starting at 2 d
262 post-transection and lasting throughout the 10 d time course (**Fig. 3C**) (ANOVA of peak
263 amplitude and peak velocity over days, F=14.93 and 30.82, p=0.0001 and 0.005). For example,
264 at 7 d, the peak amplitude of movements in response to 1000 ms illumination increased in 8/9
265 mice to on average 146% of baseline values (13.88° to 20.32°; ANOVA of 1000 ms peak
266 amplitude responses over days, F=4.55, p=0.0001), and the responses to 5 ms stimuli
267 increased by 505% of baseline (**Fig. 3C, left**) (2.75° to 13.90°; ANOVA of 5 ms peak amplitude
268 responses, F=45.01, p<2.2e-16). Peak velocity of evoked whisker movements showed similarly
269 dramatic increases. For example, at 7 d post-lesion, the peak velocity of movements in
270 response to 5 ms stimuli increased until it was indistinguishable from the velocity of movements

evoked by 1000 ms stimuli (**Fig. 3C, middle**) (834.17°/s for 5 ms stimuli, 991.49°/s for 1000 ms stimuli), indicating increased sensitivity of denervated whisker pad muscle. We further analyzed the fatigability (or adaptation) of evoked movements by measuring the persistence index of responses to 1000 ms stimuli (the ratio of final amplitude to peak amplitude; see inset in **Fig. 3C, right**). Increased persistence index indicates less fatigability to the step illumination. Persistence index increased starting 2 d post-lesion in 7/9 mice to 254% of baseline values (**Fig. 3C, right**) (0.3012 to 0.7655; ANOVA of persistence index over days, $F=27.73$, $p<2.2e-16$). Results for 10 Hz pulsed illumination were similar to the 1000 ms step illumination (**Supplemental Figure 1**; goo.gl/sWRNLU). Further comparison of 7 d and pre-lesion response duration families showed increased peak amplitudes especially for short duration stimuli (**Fig. 3D, left**), indicating reduced threshold due to increased sensitivity. Similar or even more dramatic effects were evident for peak velocity (**Fig. 3D, middle**). Parallel experiments in the same mice tracked whisker retractions evoked by illumination of the caudal retraction area (Park et al 2016) and found increased sensitivity, but not amplitude or velocity, and minimal changes in fatigability (**Supplemental Fig. 2**; goo.gl/3SDp8q), suggesting that many of the results are unique to whisker protractions. Finally, we summarized the effects of denervation on nerve- and muscle-evoked whisker protractions by comparing the changes in peak amplitude and peak velocity (24 h in ChAT-ChR2 and 7 d in Emx1-ChR2 mice). Nerve- and muscle-evoked whisker movements change in opposite directions after facial nerve transection: nerve-evoked responses were abolished by 24 h, while muscle-evoked responses increased in amplitude and velocity (**Fig. 3D, right**). The velocity of pre-lesion optogenetic muscle-evoked whisker movements was less than nerve-evoked movements (t-test of the peak velocity of pre-lesion ChAT-ChR2 and pre-lesion Emx1-ChR2 mice, $t=3.21$, $p=0.007$), but increased at 7 d post-lesion to approximately 1000˚/s, similar to the fastest pre-lesion nerve-evoked whisker movements (t-test of the peak velocity of pre-lesion ChAT-ChR2 and 7 d Emx1-ChR2 mice, $t=0.28$, $p=0.78$). Together these results indicate that denervated whisker pad protraction muscles undergo marked increases in movement capacity, including increased amplitude, velocity and sensitivity, and decreased fatigability.

Transcriptome of denervated muscle. To determine transcriptional changes underlying denervation-induced enhanced muscle function, we performed RNA-seq analysis of denervated and sham-denervated whisker pad tissue at 1, 3, and 7 d after facial nerve lesion. We calculated the differential expression of transcripts using the Kallisto/Sleuth pipeline (Bray et al 2016) and gene ontology (GO) using clusterProfiler (Pimentel et al 2017). Differentially

305 expressed transcripts were evaluated with an experiment-wide Likelihood Ratio Test (LRT) to
306 account for multiple measurements. Injury- and day-specific Wald test results that showed at
307 least a 2-fold change (FC), and were filtered by transcripts previously identified as differentially
308 expressed from LRT, were used to classify the changes in transcript levels across days
309 (Methods). After denervation, 389 transcripts were differentially expressed in whisker pad, with
310 increased expression between 1 to 3 and 7 d (**Fig. 4A**). We compared these whisker pad data
311 with a published RNA-seq dataset from the atrophy-prone soleus muscle at 3 d after
312 denervation (Macpherson et al 2015). 759 transcripts were determined to be differentially
313 expressed in injured soleus. 63 of 692 transcripts were commonly regulated between whisker
314 pad and soleus at 3 d after denervation, 629/692 were unique to one of the two models, and no
315 transcripts were regulated with at least a 2 FC in opposite directions (**Fig. 4B**). Notably, there
316 was limited overlap in GO terms and many differences (**Fig. 4C**). We further analyzed genes
317 from the cell component ontology, focusing on selected terms of interest. These are shown as
318 heatmaps of normalized expression levels at days 1, 3 and 7 d for whisker pad and day 3 for
319 soleus (transcript levels were normalized by z-score across all conditions). While genes related
320 to atrophy and cholinergic receptors, for example, were similarly upregulated in whisker pad and
321 soleus muscle, there were a number of differences, such as the expression of key ion channel
322 and contractile fiber genes (**Fig. 4D**). More complete lists are presented in **Supplemental Fig. 3**
323 (goo.gl/Afe8BE) and the full dataset can be found at GEO with accession GSE121590. These
324 comprehensive transcriptome-level data from denervated whisker pad muscle represent a key
325 basis for further understanding the enhanced functional changes we have observed.
326
327
328 **DISCUSSION**
329 We determined the functional and transcriptomic changes of mouse whisker pad that result from
330 facial motor nerve denervation. To our knowledge, our results represent the first demonstration
331 of enhanced functional properties of paralyzed whisker pad muscles, and provide a novel RNA-
332 seq dataset of the transcriptomic changes underlying this process. Our study has important
333 implications for developing future treatments for the paralysis that occurs in debilitating
334 disorders such as nerve damage and lower motor neuron degenerative diseases.
335
336 **Functional changes in nerve and muscle revealed by peripheral optogenetic stimulation**
337 In the days following motor nerve transection, the distal cut nerve undergoes a process of
338 Wallerian degeneration, leaving neuromuscular synaptic terminals transiently intact before

339 complete denervation (Tricaud & Park 2017). We used the ability to non-invasively induce
340 whisker movements longitudinally over days to measure changes in the functional properties of
341 facial nerve and whisker pad muscle throughout this process. Optogenetic stimulation of the
342 distal cut end of the facial nerve continued to produce movements for up to 24 h but degraded
343 thereafter, consistent with the time course of Wallerian degeneration (Tricaud & Park 2017).
344 After 24 h, the functional changes that occur in muscle can be attributed to the intrinsic muscle
345 changes in response to the denervation-induced loss of cholinergic input. Most muscles
346 respond to this situation with atrophy and loss of function, as evidenced by a large body of work
347 (Carlson 2014, Thesleff 1974, Wu et al 2014). A recent study that used optogenetic stimulation
348 of triceps surae muscle found more than 50% loss of both force generation and cross-sectional
349 area by 3 d after sciatic nerve lesion (Magown et al 2015). Based on these results, we expected
350 that facial nerve lesion would result in loss of whisker pad muscle function and reduced whisker
351 movements. However, we found the opposite effect. Two days after facial nerve transection, the
352 same optogenetic light stimuli applied to whisker pad muscle produced large amplitude and
353 faster whisker movements with less fatigue. Remarkably, brief light stimuli that produced no
354 movements before denervation became highly effective. For example, the response to a 5 ms
355 stimulus became near maximal and indistinguishable from the strongest (1000 ms) stimulus,
356 whereas there was no response to the 5 ms stimulus before denervation. These gain-of-function
357 changes lasted at least 10 d after denervation (the length of our study) with no indication of
358 reversal, suggesting that it is unlikely we simply missed a delayed loss-of-function response.
359 Rather, it is more likely that whisker pad muscles respond to denervation in a distinct way
360 compared to other muscle types. Our gene profiling results (below) reveal many differences with
361 the atrophy-prone soleus muscle, further supporting this idea. Importantly, expression levels of
362 ChR2 from whisker pad tissue in Emx1-ChR2 mice did not increase after facial nerve
363 transection (Supplemental Fig. 4; goo.gl/sb75Qd), ruling out the possibility that increased ChR2
364 expression led to the functional changes that we observed.
365
366 **Fasciculations, atrophy, and excitability**
367 Fasciculations (also known as fibrillations) are small-amplitude spontaneous muscle twitches
368 that commonly occur after denervation (Wu et al 2014). Fasciculations are caused by
369 oscillations in the membrane potential of muscle cells that result from denervation-induced
370 changes in the intrinsic excitability of muscle cells, including tonic membrane depolarization and
371 altered sodium and potassium conductances (Salafsky et al 1968, Thesleff & Ward 1975). In the
372 rodent whisker system, fasciculations can be precisely measured after facial nerve transection

373 by noninvasive video monitoring of the paralyzed whiskers, and furthermore are a useful
374 indicator of the state of denervation because they are abolished by reinnervation (Heaton &
375 Kobler 2005). It is tempting to speculate that fasciculations could help protect denervated
376 muscle from atrophy by providing constant excitation, but because fasciculations occur even in
377 muscles that show loss of function, the relationship between fasciculations and resilience is still
378 unclear and may vary between different muscle types. It is possible that the strength of
379 fasciculations is greater in whisker pad compared to other muscles, or that additional functional
380 or genetic factors are involved in counteracting loss of function. The relationship between
381 fasciculations, excitability, and resilience to atrophy will need to be determined in future studies.
382

383 **Strategies for stimulation of paralyzed muscle**

384 Only a few studies have demonstrated direct control of muscle via muscle-specific expression of
385 optogenetic actuators (Bruegmann et al 2015, Bryson et al 2014, Magown et al 2015, Park et al
386 2016). The optogenetic approach has major advantages over currently available technology for
387 restoration of movement. One of the advantages is the direct and safe stimulation of muscle in
388 the absence of nerve. This is different than functional electrical stimulation (FES), a commonly
389 used method in the clinic (Doucet et al 2012, Ho et al 2014, Peckham & Knutson 2005),
390 because FES depends on nerve rather than muscle stimulation. A critical limitation of FES is the
391 presence and viability of nerve, which may be compromised in cases of severe damage or
392 degenerative diseases. The high electrical currents needed in these cases can cause problems
393 such as tissue damage, non-specific spread across muscle groups, and discomfort (Plenk
394 2011). Thus, the ability of optogenetics to non-invasively stimulate muscle in the absence of
395 nerve is a major advantage compared to current electrical approaches or optogenetic nerve
396 stimulation approaches (Llewellyn et al 2010), and indeed could be the only viable approach to
397 restore the function of muscle after severe injuries or diseases that result in complete and
398 permanent denervation. There are still significant issues that need to be solved in order to
399 translate optogenetics to the clinic, including the expression of light-sensitive proteins in tissue
400 of interest using viral vectors and appropriate hardware for light delivery (Fenno et al 2011,
401 Montgomery et al 2016, Yizhar et al 2011), and thus these remain active areas of research.
402

403 **Transcriptome of denervated muscle**

404 Discovering the expression changes that occur in denervated muscle is an important goal for
405 developing strategies to restore muscle function. We used RNA-seq to detect and quantify
406 transcript levels changing over time following denervation. In particular, our objective was to

understand the unique transcriptomic landscape of the denervated whisker pad, which shows enhanced muscle function, compared to other muscle samples that show loss of function. Thus, by comparing our dataset with an existing dataset from atrophy-prone soleus muscle at a matching 3 d time point after denervation (Macpherson et al 2015), we identified unique features of the denervated whisker pad. Our results indicate that expression of several key genes was regulated in the same direction in both whisker pad and soleus (either up- or both down-regulated), while many others showed differential expression as we would have predicted based on functional differences. For example, expression of the atrophy-related genes *Myog* and *Mtor*, and *Chrn* nicotinic cholinergic receptor family genes were upregulated in both whisker pad and soleus. However, there were prominent differences in expression of genes for ion channels and contractile fibers. For example, the *Kcn* family of voltage-gated potassium channels showed several instances of upregulation in whisker pad and downregulation in soleus, and vice versa. Similarly, slow-twitch (type II) contractile fibers, including *Myom3* and *Myh8*, were upregulated in whisker pad and downregulated in soleus, consistent with fiber-type switches after denervation. It is likely that the differences in expression of ion channels and contractile fibers at least partly explain the distinct functional responses of these muscles to denervation. For example, the upregulation of slow-twitch fibers in whisker pad is consistent with the striking decrease in fatigability that we observed (Figure 3). Changes in expression of voltage-gated ion channels, including potassium channels, sodium channels, and many others, can result in membrane potential depolarization, oscillations, and changes in the waveform of the action potential. These features likely relate to the changes in optogenetically evoked whisker movements that we measured, including increased sensitivity, amplitude, and velocity. The detailed relationship between ion channel and contractile fiber expression with the functional changes requires further investigation. Another outstanding question is how changes in excitability relate to susceptibility to atrophy. One possibility is that atrophy-related genetic programs are activated in all denervated muscle types, but additional changes in excitability that lead to enhanced function in some muscles types essentially counteract this process. Since our experiments focused on functional changes in muscle responses as measured with optogenetic stimulation and video recording of whisker movements, further studies are needed to determine whether atrophy occurred on the level of individual muscle fibers.

It should be noted that our samples were limited to the rostral protraction area of the whisker pad. At this location, the spot of light activates primarily the extrinsic protractor muscles pars media superior and pars media inferior of *M. nasolabialis profundus* and also the intrinsic

441 follicular muscles (Haidarliu et al 2010, Jin et al 2004, Park et al 2016). In the future, it would be
442 interesting to compare RNA-seq results with the caudal retraction area, which showed
443 increased sensitivity but more subtle changes in amplitude and fatigability (Supplemental Figure
444 2; goo.gl/3SDp8q), to identify further links between changes in gene expression and movement
445 phenotypes. It would also be important in future work to obtain more complete datasets
446 comparing functional and transcriptomic results from several muscles types. This would help
447 address drawbacks in the comparison of our RNA-seq dataset with published data from soleus
448 (Macpherson et al 2015), including that the samples were obtained from mice of different ages,
449 and that our biopsied samples included both skin and muscle tissue. Future work could also
450 directly relate transcriptomic and functional data by performing genetic analysis of the same
451 subjects used for the optogenetic measures, which was not done here.
452
453 **Conclusion**
454 In conclusion, our combined functional and transcriptomic results have implications for future
455 work on the restoration of movement following nerve damage or motoneuron degeneration. The
456 unique properties of denervated whisker pad muscles that we have identified could inform future
457 genetic strategies to restore muscle function after nerve injury or motoneuron degeneration in
458 various neuromuscular systems.
459
460

461 **REFERENCES**

462 Bray, N.L., Pimentel, H., Melsted, P., and Pachter, L. (2016). Near-optimal probabilistic
463 RNA-seq quantification. Nature biotechnology 34, 525-527.

464 Bruegmann, T., van Bremen, T., Vogt, C.C., Send, T., Fleischmann, B.K., and Sasse, P.
465 (2015). Optogenetic control of contractile function in skeletal muscle. Nature
466 communications 6, 7153.

467 Bryson, J.B., Machado, C.B., Crossley, M., Stevenson, D., Bros-Facer, V., Burrone, J.,
468 Greensmith, L., and Lieberam, I. (2014). Optical control of muscle function by
469 transplantation of stem cell-derived motor neurons in mice. Science 344, 94-97.

470 Carlson, B.M. (2014). The Biology of Long-Term Denervated Skeletal Muscle. European
471 journal of translational myology 24, 3293.

472 Clack, N.G., O'Connor, D.H., Huber, D., Petreanu, L., Hires, A., Peron, S., Svoboda, K.,
473 and Myers, E.W. (2012). Automated tracking of whiskers in videos of head fixed rodents.
474 PLoS computational biology 8, e1002591.

475 Doucet, B.M., Lam, A., and Griffin, L. (2012). Neuromuscular electrical stimulation for
476 skeletal muscle function. The Yale journal of biology and medicine 85, 201-215.

477 Fenno, L., Yizhar, O., and Deisseroth, K. (2011). The Development and Application of
478 Optogenetics. Annual Review of Neuroscience 34, 389-412.

479 Griffin, G.R., and Kim, J.C. (2011). Potential of an electric prosthesis for dynamic facial
480 reanimation. Otolaryngology--head and neck surgery : official journal of American
481 Academy of Otolaryngology-Head and Neck Surgery 145, 365-368.

482 Hadlock, T.A., Heaton, J., Cheney, M., and Mackinnon, S.E. (2005). Functional recovery
483 after facial and sciatic nerve crush injury in the rat. Archives of facial plastic surgery 7, 17-
484 20.

485 Haidarliu, S., Kleinfeld, D., Deschenes, M., and Ahissar, E. (2015). The Musculature That
486 Drives Active Touch by Vibrissae and Nose in Mice. Anatomical record (Hoboken, NJ :
487 2007) 298, 1347-1358.

488 Haidarliu, S., Simony, E., Golomb, D., and Ahissar, E. (2010). Muscle architecture in the
489 mystacial pad of the rat. Anatomical record (Hoboken, NJ : 2007) 293, 1192-1206.

490 Heaton, J.T., and Kobler, J.B. (2005). Use of muscle fibrillation for tracking nerve
491 regeneration. Muscle Nerve 31, 235-241.

492 Heaton, J.T., Sheu, S.H., Hohman, M.H., Knox, C.J., Weinberg, J.S., Kleiss, I.J., and
493 Hadlock, T.A. (2014). Rat whisker movement after facial nerve lesion: evidence for
494 autonomic contraction of skeletal muscle. Neuroscience 265, 9-20.

495 Ho, C.H., Triolo, R.J., Elias, A.L., Kilgore, K.L., DiMarco, A.F., Bogie, K., Vette, A.H., Audu,
496 M.L., Kobetic, R., Chang, S.R., et al. (2014). Functional electrical stimulation and spinal
497 cord injury. Physical medicine and rehabilitation clinics of North America 25, 631-654, ix.

498 Jin, T.E., Witzemann, V., and Brecht, M. (2004). Fiber types of the intrinsic whisker muscle
499 and whisking behavior. J Neurosci 24, 3386-3393.

500 Jones, R., and Vrbova, G. (1974). Two factors responsible for the development of
501 denervation hypersensitivity. J Physiol 236, 517-538.

502 Lee, C.R., and Margolis, D.J. (2016). Pupil Dynamics Reflect Behavioral Choice and
503 Learning in a Go/NoGo Tactile Decision-Making Task in Mice. Frontiers in behavioral
504 neuroscience 10, 200.

505 Llewellyn, M.E., Thompson, K.R., Deisseroth, K., and Delp, S.L. (2010). Orderly
506 recruitment of motor units under optical control in vivo. Nature medicine 16, 1161-1165.

507 Lomo, T., and Rosenthal, J. (1972). Control of ACh sensitivity by muscle activity in the rat.
508 J Physiol 221, 493-513.

509 Macpherson, P.C., Farshi, P., and Goldman, D. (2015). Dach2-Hdac9 signaling regulates
510 reinnervation of muscle endplates. Development (Cambridge, England) 142, 4038-4048.

511 Madisen, L., Mao, T., Koch, H., Zhuo, J.M., Berenyi, A., Fujisawa, S., Hsu, Y.W., Garcia,
512 A.J., 3rd, Gu, X., Zanella, S., et al. (2012). A toolbox of Cre-dependent optogenetic
513 transgenic mice for light-induced activation and silencing. Nat Neurosci 15, 793-802.

514 Magown, P., Shettar, B., Zhang, Y., and Rafuse, V.F. (2015). Direct optical activation of
515 skeletal muscle fibres efficiently controls muscle contraction and attenuates denervation
516 atrophy. Nature communications 6, 8506.

517 Montgomery, K.L., Iyer, S.M., Christensen, A.J., Deisseroth, K., and Delp, S.L. (2016).
518 Beyond the brain: Optogenetic control in the spinal cord and peripheral nervous system.
519 Science translational medicine 8, 337rv335.

520 Nelson, P.G. (1969). Functional consequences of tenotomy in hind limb muscles of the
521 cat. J Physiol 201, 321-333.

522 Olmstead, D.N., Mesnard-Hoaglin, N.A., Batka, R.J., Haulcomb, M.M., Miller, W.M., and
523 Jones, K.J. (2015). Facial nerve axotomy in mice: a model to study motoneuron response
524 to injury. Journal of visualized experiments : JoVE, e52382.

525 Park, S., Bandi, A., Lee, C.R., and Margolis, D.J. (2016). Peripheral optogenetic
526 stimulation induces whisker movement and sensory perception in head-fixed mice. Elife 5.

527 Peckham, P.H., and Knutson, J.S. (2005). Functional electrical stimulation for
528 neuromuscular applications. Annual review of biomedical engineering 7, 327-360.

529 Pimentel, H., Bray, N.L., Puente, S., Melsted, P., and Pachter, L. (2017). Differential
530 analysis of RNA-seq incorporating quantification uncertainty. Nature methods 14, 687-690.

531 Plenk, H., Jr. (2011). The role of materials biocompatibility for functional electrical
532 stimulation applications. Artificial organs 35, 237-241.

533 Rossi, J., Balthasar, N., Olson, D., Scott, M., Berglund, E., Lee, C.E., Choi, M.J., Lauzon,
534 D., Lowell, B.B., and Elmquist, J.K. (2011). Melanocortin-4 receptors expressed by

535 cholinergic neurons regulate energy balance and glucose homeostasis. Cell metabolism
536 13, 195-204.

537 Salafsky, B., Bell, J., and Prewitt, M.A. (1968). Development of fibrillation potentials in
538 denervated fast and slow skeletal muscle. The American journal of physiology 215, 637-
539 643.

540 Sellin, L.C., and Thesleff, S. (1980). Alterations in membrane electrical properties during
541 long-term denervation of rat skeletal muscles. Acta physiologica Scandinavica 108, 243-
542 246.

543 Thesleff, S. (1974). Trophic functions of the neuron. II. Denervation and regulation of
544 muscle. Physiological effects of denervation of muscle. Annals of the New York Academy
545 of Sciences 228, 89-104.

546 Thesleff, S., and Ward, M.R. (1975). Studies on the mechanism of fibrillation potentials in
547 denervated muscle. J Physiol 244, 313-323.

548 Tricaud, N., and Park, H.T. (2017). Wallerian demyelination: chronicle of a cellular
549 cataclysm. Cellular and molecular life sciences : CMLS 74, 4049-4057.

550 Wu, P., Chawla, A., Spinner, R.J., Yu, C., Yaszemski, M.J., Windebank, A.J., and Wang,
551 H. (2014). Key changes in denervated muscles and their impact on regeneration and
552 reinnervation. Neural regeneration research 9, 1796-1809.

553 Yizhar, O., Fenno, Lief E., Davidson, Thomas J., Mogri, M., and Deisseroth, K. (2011).
554 Optogenetics in Neural Systems. Neuron 71, 9-34.

555

556

557 **Acknowledgements**

558 Supported in part by grants from the National Institutes of Health (R01NS094450) and the New
559 Jersey Commission on Brain Injury Research (CBIR16IRG032) to DJM. AU was a member of
560 the NeuroSURP program (NIH R25NS105143). We thank S. Olga Yiantsos, Ridhima Sakhuja,
561 Fizza Fahim, Sydney Terris, Hill Chang, Jennifer Fang and Emefa Ocansey for assistance with
562 experiments. We thank RUCDR Infinite Biologics staff for collection of RNA-seq data and the
563 Office of Advanced Research Computing (OARC) at Rutgers, The State University of New
564 Jersey for providing access to the Perceval cluster and associated research computing
565 resources that have contributed to the results reported here with support from NIH
566 (S10OD012346). URL: http://oarc.rutgers.edu. Author contributions: AB, TJV, AU, RPH, CRL,
567 DJM designed experiments, AB, AU, CRL, MRS, DJM performed experiments, TJV, AB, RPH
568 analyzed data, DJM drafted manuscript with input from all authors.

569

570

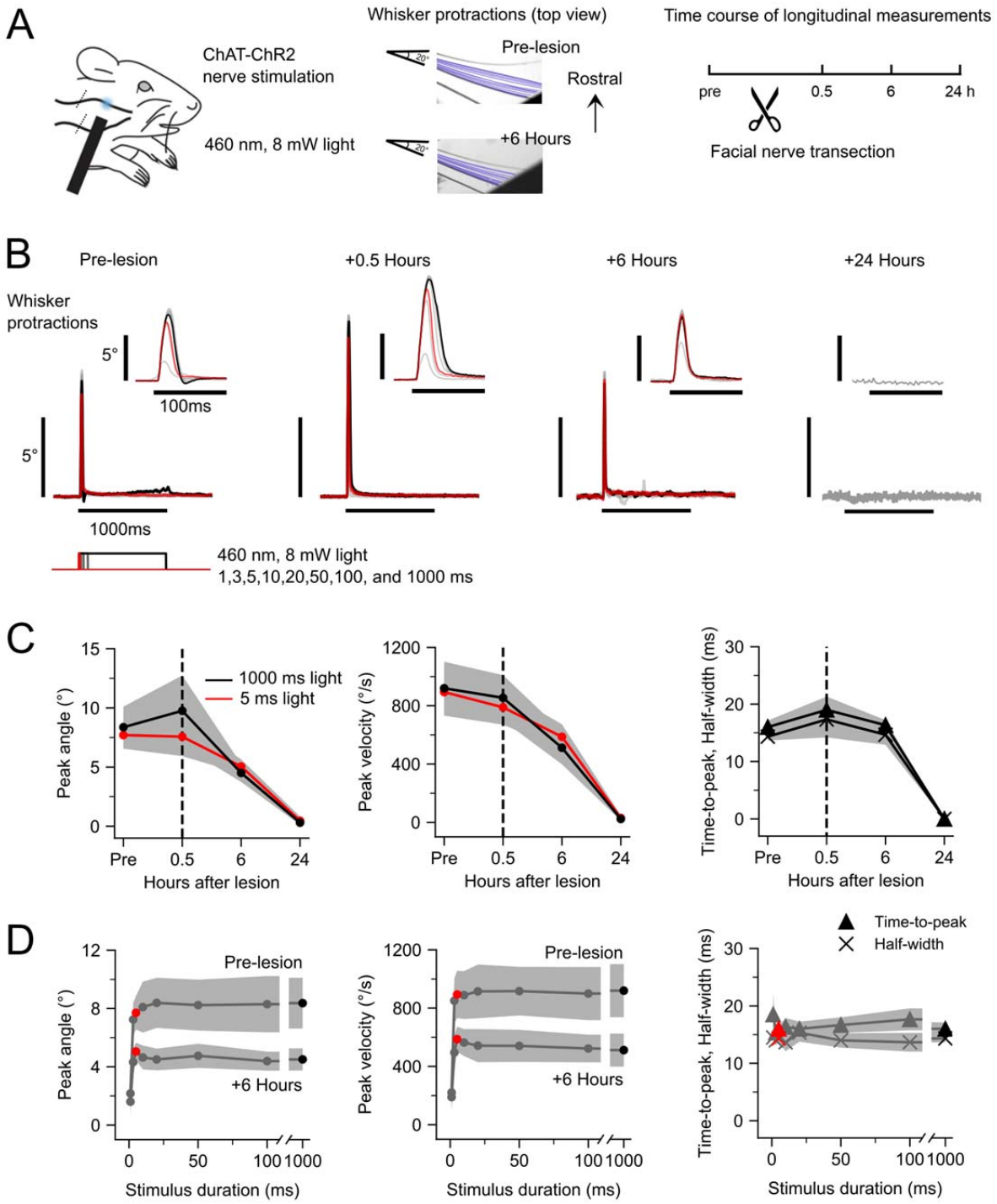

571
572 **Figure 1. Functional degradation of facial nerve.**

(A) Optogenetic nerve paradigm. Left: Schematic of transdermal facial nerve illumination in ChAT-ChR2 mice. Position of optogenetic illumination indicated with blue spot. Position of nerve transection indicated with diagonal lines crossing buccal and marginal nerve branches caudal to illumination site. Middle: Frame-by-frame position of one tracked whisker in an example subject in response to a 1000 ms, 8 mW pulse of 460 nm LED illumination pre-lesion and 6 h post-lesion. Right: Experimental timeline.
(B) Whisker protractions evoked by optogenetic nerve stimulation from an example mouse at various times relative to nerve transection. Each trace is the average of 10 responses to a different duration of illumination at 8 mW. Stimuli are 1, 3, 5, 10, 20, 50, 100, 1000 ms, with 5 ms (red) and 1000 ms (black) highlighted. Insets show the same traces on an expanded time scale.
(C) Time course of peak amplitude (left), peak velocity (middle), time-to-peak and half-width (right) of whisker protractions in response to 5 ms (red) and 1000 ms (black) light stimuli. In all cases, responses were significantly abolished by 24 h post-transection (see text for further statistics). Values are mean ± SEM; n=6 mice.
(D) Pre-lesion and 6 h response duration families for peak amplitude (left) and peak velocity (middle). Pre-lesion response duration families for time-to-peak and half-width (right). Red circle, 5 ms; black circle, 1000 ms stimuli. Values are mean ± SEM; n=6 mice.

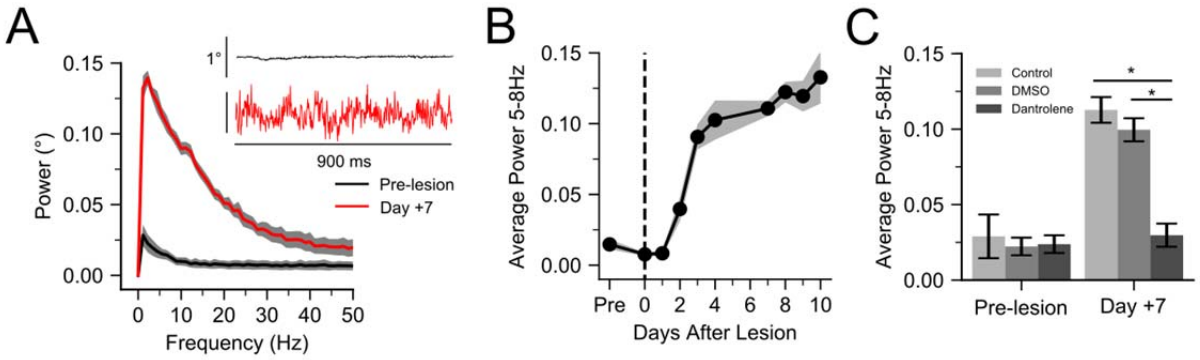

Figure 2. Muscle origin of fasciculations.
(A) Power spectra of spontaneous whisker fasciculations at baseline and 7 d post-lesion. Inset, examples of spontaneous whisker movements at baseline and 7 d.
(B) Time course of fasciculation strength (mean ± SEM 5-8 Hz power; n = 9, Emx1-ChR2 mice).
(C) Effects of RyR1 antagonist dantrolene (1 mM). Bar graphs show mean ± SEM of 5-8 Hz power (n = 5, Emx1-ChR2 mice); * indicates $p < 0.05$.

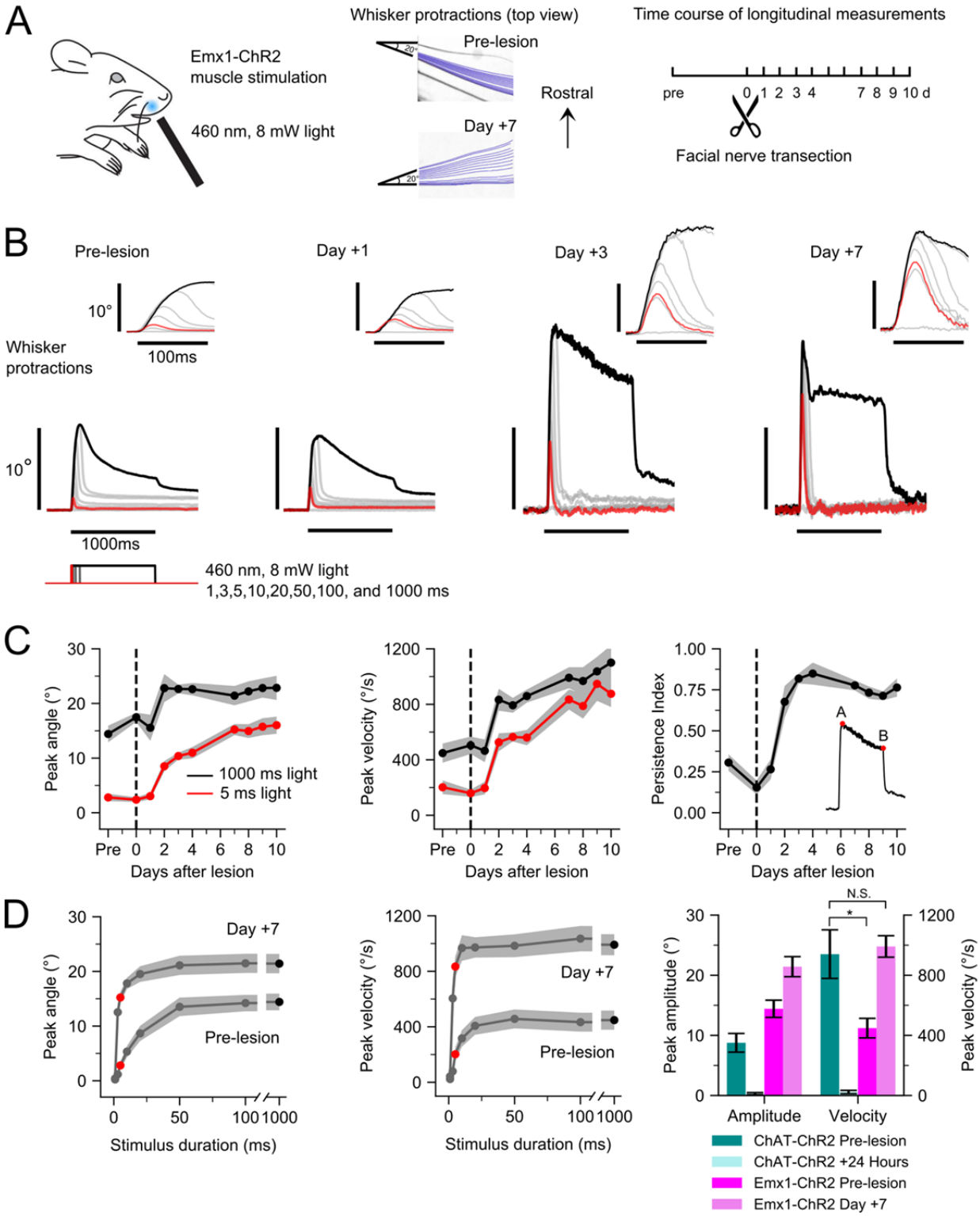

Figure 3. Functional enhancement of denervated muscle.

(A) Optogenetic muscle paradigm. Left: Schematic of transdermal muscle illumination in Emx1-ChR2 mice. Position of optogenetic illumination indicated with blue spot. Middle: Frame-by-frame position of one

604 tracked whisker in an example subject in response to a 1000 ms, 8 mW pulse of 460 nm LED illumination
605 pre-lesion and 7 d post-lesion. Right: Experimental timeline.
606 **(B)** Whisker protractions evoked by optogenetic muscle stimulation from an example mouse at various
607 times relative to nerve transection. Each trace is the average of 10 responses to a different duration of
608 illumination at 8 mW. Stimuli are 1, 3, 5, 10, 20, 50, 100, 1000 ms, with 5 ms (red) and 1000 ms (black)
609 highlighted. Insets show the same traces on an expanded time scale.
610 **(C)** Time course of peak amplitude (left) and peak velocity (middle) of whisker protractions in responses
611 to 5 ms (red) and 1000 ms (black) light stimuli. Time course of persistence index for 1000 ms stimulus
612 (right); inset shows that persistence index is the ratio of response amplitude at 1000 ms to peak
613 amplitude (B/A). Values are mean ± SEM; n=9 mice.
614 **(D)** Pre-lesion and 7 d response duration families for peak amplitude (left) and peak velocity (middle).
615 Red circle, 5 ms; black circle, 1000 ms stimuli. Right: Summary data comparing amplitude and velocity
616 changes for ChAT-ChR2 (blues) and Emx1-ChR2 mice (magentas) in response to 1000 ms stimuli. T-
617 tests compare velocity values for pre-lesion ChAT-ChR2 with pre-lesion Emx1-ChR2, and pre-lesion
618 ChAT-ChR2 with day +7 Emx1-ChR2. Values are mean ± SEM; n=9 mice. * indicates $p<0.05$, N.S.
619 indicates not significant.

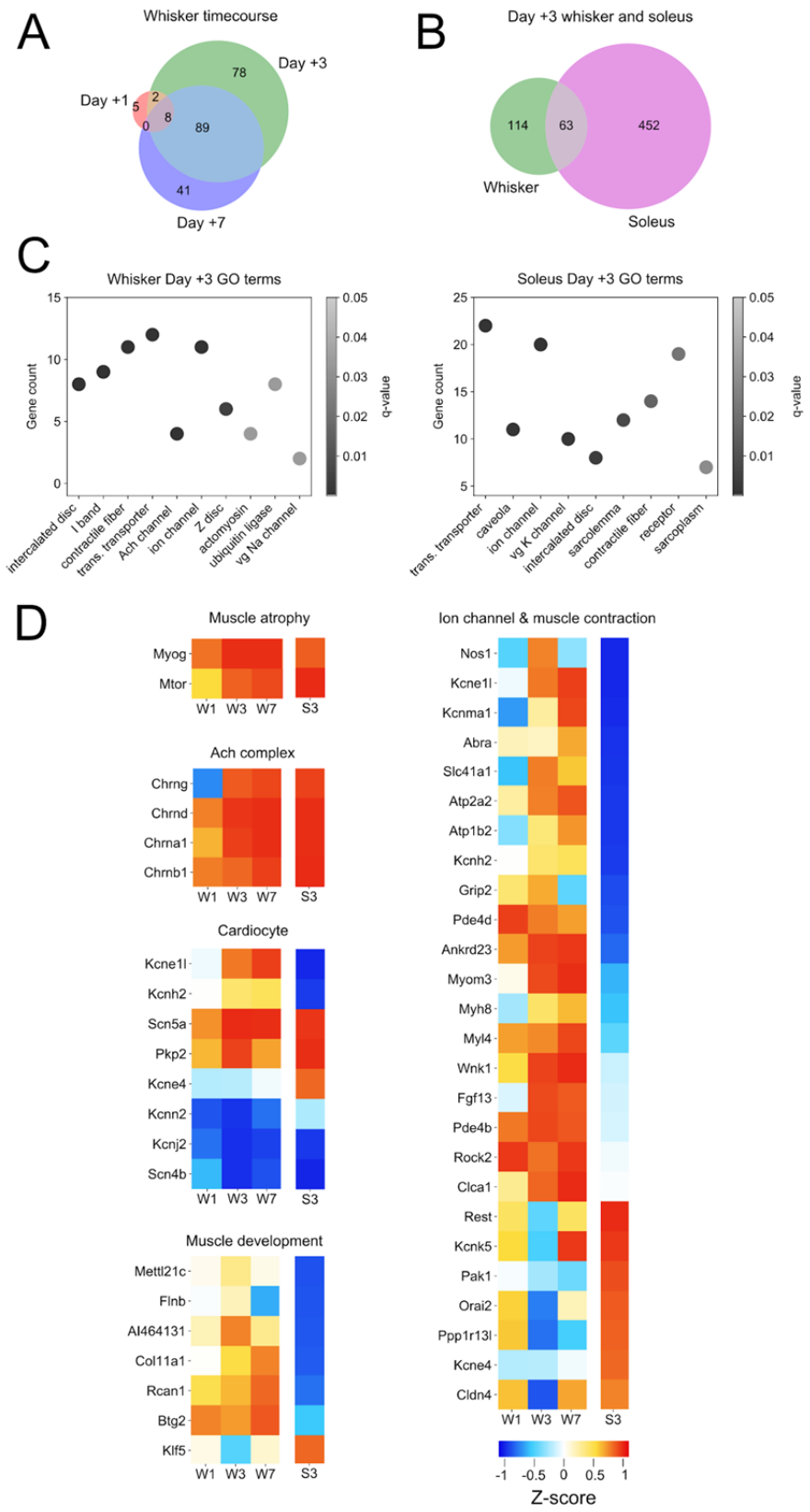

Figure 4. Transcriptome of denervated whisker pad muscle.

(A) Venn diagram of differentially expressed transcripts from whisker pad with at least ± 2-fold change (FC) at 1, 3 and 7 d post-denervation (n=3 mice at each time point).
(B) Venn diagram of differentially expressed transcripts with ± 2-FC from whisker pad and soleus at 3 d post-denervation. Soleus data in panels B, C and D is from (Macpherson et al., 2011; n=2 mice).
(C) Subset of enriched cell component GO terms for whisker pad (left) and soleus (right) at 3 d post-denervation. Identity numbers of GO terms are listed in Methods.
(D) Heatmaps of expression for gene families related to Muscle atrophy, ACh complex, Cardiocyte, Muscle development, and Ion channels & Muscle contraction. Data shown as average z-score. Columns labeled W1, W3 and W7 indicate whisker pad data from 1, 3, and 7 d post-denervation, respectively. Rightmost columns labeled S3 indicate soleus data from 3 d post denervation. For Muscle development and Ion channel & Muscle contraction groups, genes included in heatmap were limited to those that had polar directional z-scores between whisker pad and soleus at 3 d.

Data supplements are available via links in text and https://github.com/margolislab/Vajtay_Bandi_2018.

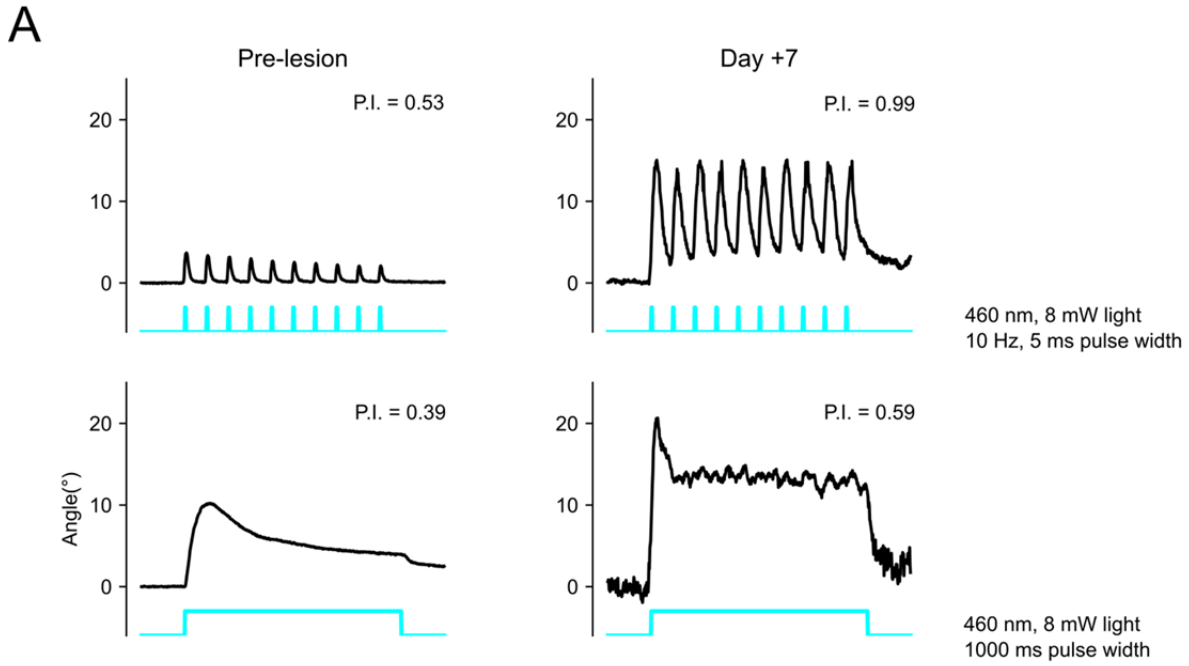

Supplemental Figure 1. Comparison of whisker protractions to 10 Hz and step illumination. **(A)** Top row shows responses to 10 Hz light stimuli (5 ms pulse width) before and 7 days after nerve transection in an example mouse. Bottom row shows responses to step illumination (1000 ms) before and 7 days after nerve transection in the same example mouse as in the top row. Each trace is a representative single trial.

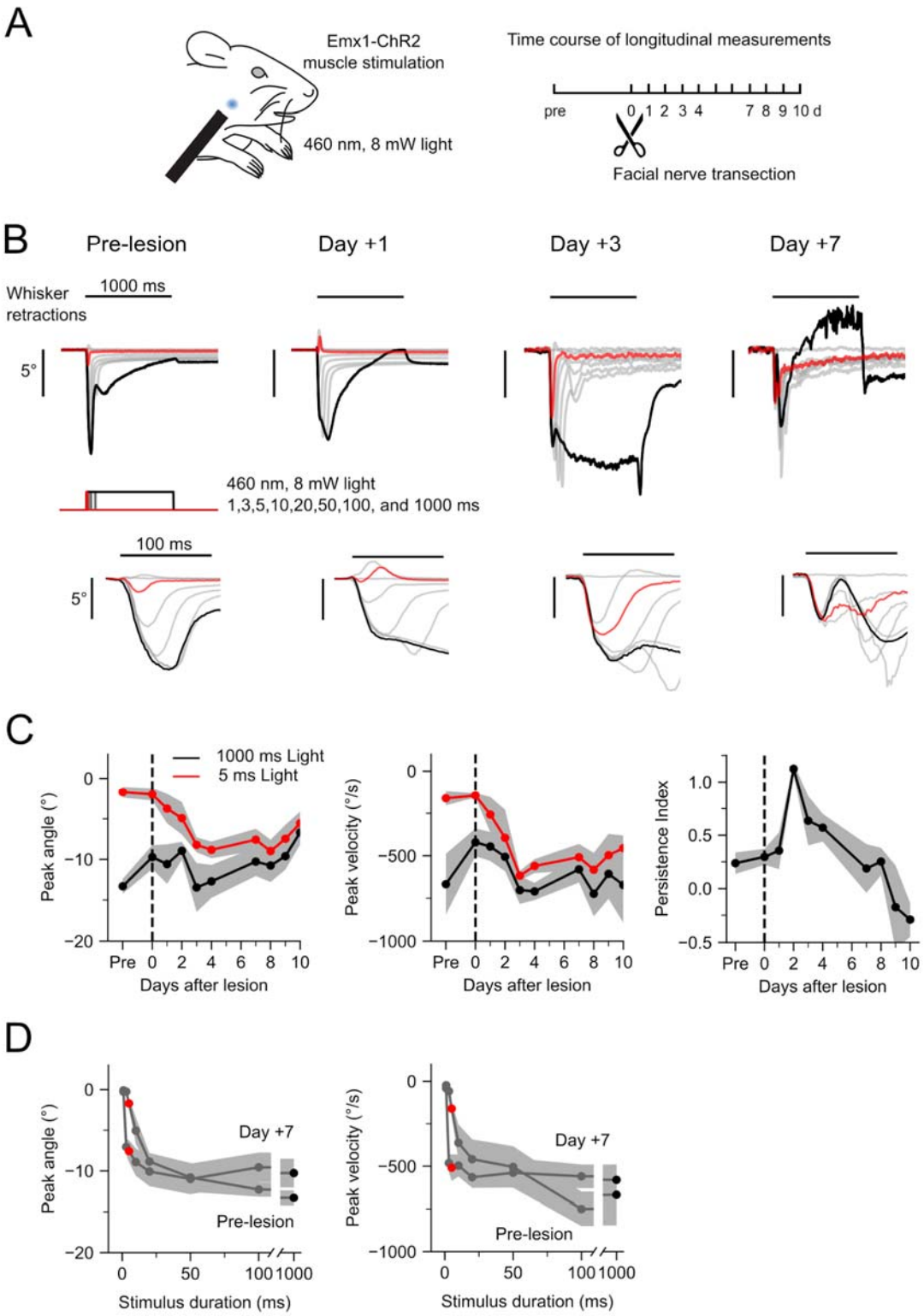

Supplemental Figure 2. Effects of denervation at caudal retraction area.
(A) Optogenetic muscle paradigm. Left: Schematic of transdermal muscle illumination in Emx1-ChR2 mice. Position of optogenetic illumination indicated with blue spot. Right: Experimental timeline.

(B) Whisker retractions evoked by optogenetic nerve stimulation from an example mouse at various times relative to nerve transection. Each trace is the average of 10 responses to a different duration of illumination at 8 mW. red, 5 ms stimulus; black, 1000 ms stimulus; gray, 1, 3, 10, 20, 50, 100 ms. Insets (below) show movements on an expanded time scale.
(C) Time course of peak amplitude (left), time course of peak velocity (middle), and time course of persistence index from 1000 ms stimuli. High persistence index indicates low fatigability. Red, 5 ms; black, 1000 ms stimuli. Values are mean ± SEM; n=9 mice.
(D) Comparison of baseline and 7 d response duration families for peak amplitude (left) and peak velocity (middle). Red, 5 ms; black, 1000 ms stimuli. Values are mean ± SEM; n=9 mice.

A

Enriched whisker Day +3 CC GO terms

GO Term	GeneRatio
intercalated disc	8/159
cell-cell contact zone	8/159
myofibril	11/159
I band	9/159
contractile fiber	11/159
sarcomere	10/159
contractile fiber part	10/159
transmembrane transporter complex	12/159
transporter complex	12/159
acetylcholine-gated channel complex	4/159
ion channel complex	11/159
cell-cell junction	13/159
filopodium membrane	3/159
Z disc	6/159
filopodium	5/159
actin-based cell projection	7/159
Cul3-RING ubiquitin ligase complex	4/159
receptor complex	9/159
actomyosin	4/159
ubiquitin ligase complex	8/159
voltage-gated sodium channel complex	2/159
leading edge membrane	5/159
invadopodium	2/159
sarcolemma	5/159

Enriched soleus Day +3 CC GO terms

GO Term	GeneRati
cell-cell junction	31/490
transmembrane transporter complex	22/490
transporter complex	22/490
caveola	11/490
ion channel complex	20/490
voltage-gated potassium channel complex	10/490
potassium channel complex	10/490
plasma membrane raft	11/490
intercalated disc	8/490
membrane raft	20/490
membrane microdomain	20/490
sarcolemma	12/490
membrane region	20/490
cell-cell contact zone	8/490
T-tubule	7/490
contractile fiber	14/490
sarcoplasmic reticulum	7/490
receptor complex	19/490
cation channel complex	13/490
sarcoplasm	7/490
sarcoplasmic reticulum membrane	4/490
contractile fiber part	12/490
voltage-gated sodium channel complex	3/490

B

Top 50 whisker pad

Gene name	transcript_id
Myog	ENSMUST00000027730.5
Scn5a	ENSMUST00000065196.12
Gdf5	ENSMUST00000040162.2
Smad3	ENSMUST00000034973.9
Hdac4	ENSMUST00000097644.8
Mlf1	ENSMUST00000061322.9
Fhl3	ENSMUST00000038684.5
Snai3	ENSMUST00000006762.6
Kbtbd13	ENSMUST00000068307.3
Chrnd	ENSMUST00000073252.8
Carns1	ENSMUST00000167055.1
Carns1	ENSMUST00000181869.2
Tbc1d4	ENSMUST00000161304.1
Kcnj2	ENSMUST00000042970.2
Adamtsl4	ENSMUST00000015994.3
Pvr	ENSMUST00000043517.7
Eda2r	ENSMUST00000037353.9
Alpk2	ENSMUST00000035548.14
Myod1	ENSMUST00000072514.2
Plekhh1	ENSMUST00000219946.1
Phkg1	ENSMUST00000200832.1
Eepd1	ENSMUST00000040677.5
Hdac9	ENSMUST00000110819.3
Kcna7	ENSMUST00000107774.2
Gadd45a	ENSMUST00000043098.8
Runx1	ENSMUST00000023673.13
Tigar	ENSMUST00000039913.8
Fn3k	ENSMUST00000026175.8
Gprc5c	ENSMUST00000053361.11
Ufsp1	ENSMUST00000052825.6
Mtch1	ENSMUST00000095427.10
Smco1	ENSMUST00000093183.3
Myf6	ENSMUST00000044210.4
Ankrd23	ENSMUST00000193083.5
Atoh8	ENSMUST00000206425.1
Eef1akmt4	ENSMUST00000115522.8
Klhl33	ENSMUST00000227271.1
Asb18	ENSMUST00000086882.7
Sec14l5	ENSMUST00000230616.1
Kcnn3	ENSMUST00000124584.3
Chrna1	ENSMUST00000028515.3
Mtch1	ENSMUST00000118366.7
Uqcc1	ENSMUST00000109636.10
Ppp1r27	ENSMUST00000026121.2
Lrrc52	ENSMUST00000036643.5
Tubb6	ENSMUST00000001513.6
Gadd45a	ENSMUST00000126194.1
Pitpnc1	ENSMUST00000040380.12
Peg3	ENSMUST00000051209.10
Stum	ENSMUST00000136521.1

Top 50 soleus

Gene name	transcript_id
Ngfr	ENSMUST00000000122.6
Fgf6	ENSMUST00000000187.6
Ccnd2	ENSMUST00000000188.11
Bcl6b	ENSMUST00000000326.11
Alox12	ENSMUST00000000329.8
Kcnn3	ENSMUST00000000811.7
Hip1r	ENSMUST00000000939.14
Col6a1	ENSMUST00000001147.4
Col6a2	ENSMUST00000001181.12
Tubb6	ENSMUST00000001513.6
Col1a1	ENSMUST00000001547.7
Aif1l	ENSMUST00000001920.12
Abcd1	ENSMUST00000002084.13
Ppm1j	ENSMUST00000002298.6
Zim1	ENSMUST00000002336.15
Lamb1	ENSMUST00000002979.14
Abcb4	ENSMUST00000003717.12
Gstm7	ENSMUST00000004137.10
Mtfp1	ENSMUST00000004868.5
Klf5	ENSMUST00000005279.7
Nid1	ENSMUST00000005532.8
Hmox1	ENSMUST00000005548.7
Slc30a4	ENSMUST00000005952.10
Tead4	ENSMUST00000006311.12
Vwa7	ENSMUST00000007245.7
Tgfbr1	ENSMUST00000007757.14
Abhd8	ENSMUST00000008094.9
Mymk	ENSMUST00000009358.8
Dll1	ENSMUST00000014917.7
Tppp3	ENSMUST00000014990.12
Aldh1a3	ENSMUST00000015278.14
Lpl	ENSMUST00000015712.14
Adamtsl4	ENSMUST00000015994.3
Cd274	ENSMUST00000016640.7
Vtn	ENSMUST00000017488.4
Traf4	ENSMUST00000017530.3
Myh8	ENSMUST00000019625.11
Pde7b	ENSMUST00000020165.13
Igfbp3	ENSMUST00000020702.10
Adcy1	ENSMUST00000020706.4
Nrcam	ENSMUST00000020939.15
Id2	ENSMUST00000020974.6
Rrm2	ENSMUST00000020980.11
Klf11	ENSMUST00000020982.6
Ccl7	ENSMUST00000021011.2
Slc9a3r1	ENSMUST00000021077.3
Tac4	ENSMUST00000021242.4
Serpina3n	ENSMUST00000021506.5
Galnt16	ENSMUST00000021558.7
Fos	ENSMUST00000021674.6

C

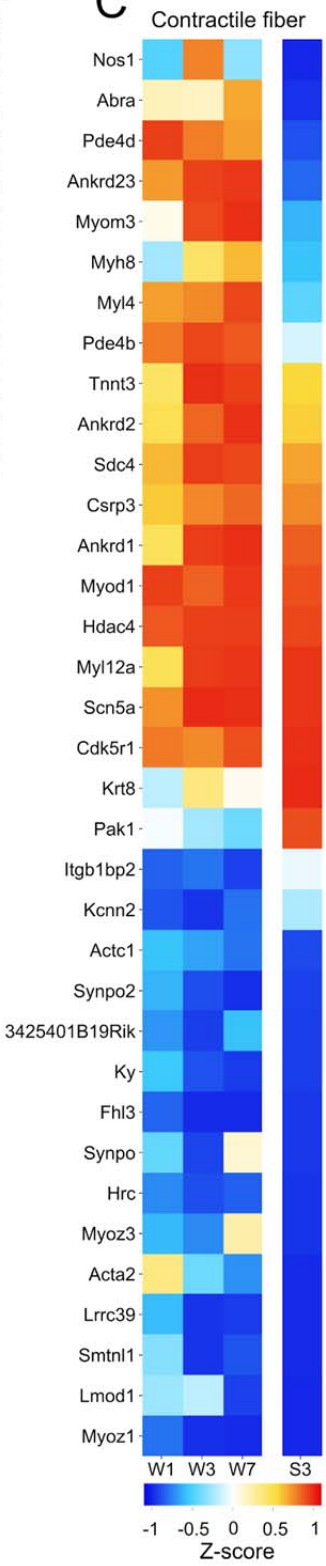

Supplemental Figure 3. Additional transcriptome data for denervated whisker pad and soleus muscle.

662 **(A)** Full lists of enriched GO terms for both whisker pad and soleus 3 d calculated from a ranked list of
663 differentially expressed ± 2-FC transcript gene IDs. All GO terms listed were significantly enriched by
664 hypergeometric test at $q<0.05$.
665 **(B)** List of top 50 significant differentially expressed transcripts for both whisker pad and soleus.
666 **(C)** Full heatmap of differentially expressed genes included in the Contractile fiber GO term. Data shown
667 as average z-score. Columns labeled W1, W3 and W7 indicate whisker pad data from 1, 3, and 7 d post-
668 denervation, respectively. Rightmost columns labeled S3 indicate soleus data from 3 d post denervation.

669

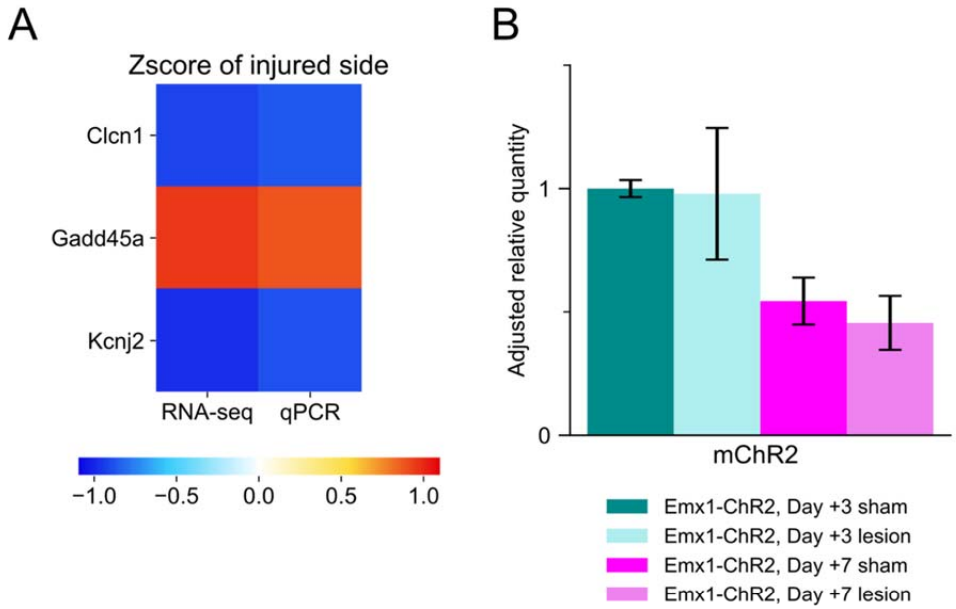

C

Name	Sequence
mClcn1_F	TACGGACTGCCCTCAGAGAA
mClcn1_R	TGGCCATATATCTGTGTTGGGT
mGadd45a_F	TGGTGACGAACCCACATTCA
mGadd45a_R	TCCATGTAGCGACTTTCCCG
mKcnj2_F	CCTGTACCAGCAACAGGACAA
mKcnj2_R	TGGGGTTCTTTTGACCAGCA
mActb_F	GGCTGTATTCCCCTCCATCG
mActb_R	CCAGTTGGTAACAATGCCATGT
mChR2_F	CCATGGGTCTGCTTGTGTCT
mChR2_R	GACCTTGACGTATCCGGTGG

670
671
672
673 **Supplemental Figure 4. qPCR validation of RNA-seq data and measurements of ChR2 expression.**
674 **(A)** Heatmap of differential expression of Clcn1, Gadd45a, and Kcnj2 from 3 d whisker pad for RNA-seq
675 (left column) and qPCR (right column). qPCR values were normalized to ActB expression.
676 **(B)** qPCR data comparing ChR2 expression levels in sham and lesioned whisker pad tissue from Emx1-
677 ChR2 mice. Bars (errorbars) represent mean (± SEM) data from left (sham) and right (lesion) whisker
678 pads from day 3 (n=3 mice) and day 7 (n=2 mice) after lesion. One of the five subjects included was
679 unlesioned. No increases were detected at 3 d and 7 d post-lesion.
680 **(C)** Name and sequence of primers used for qPCR.

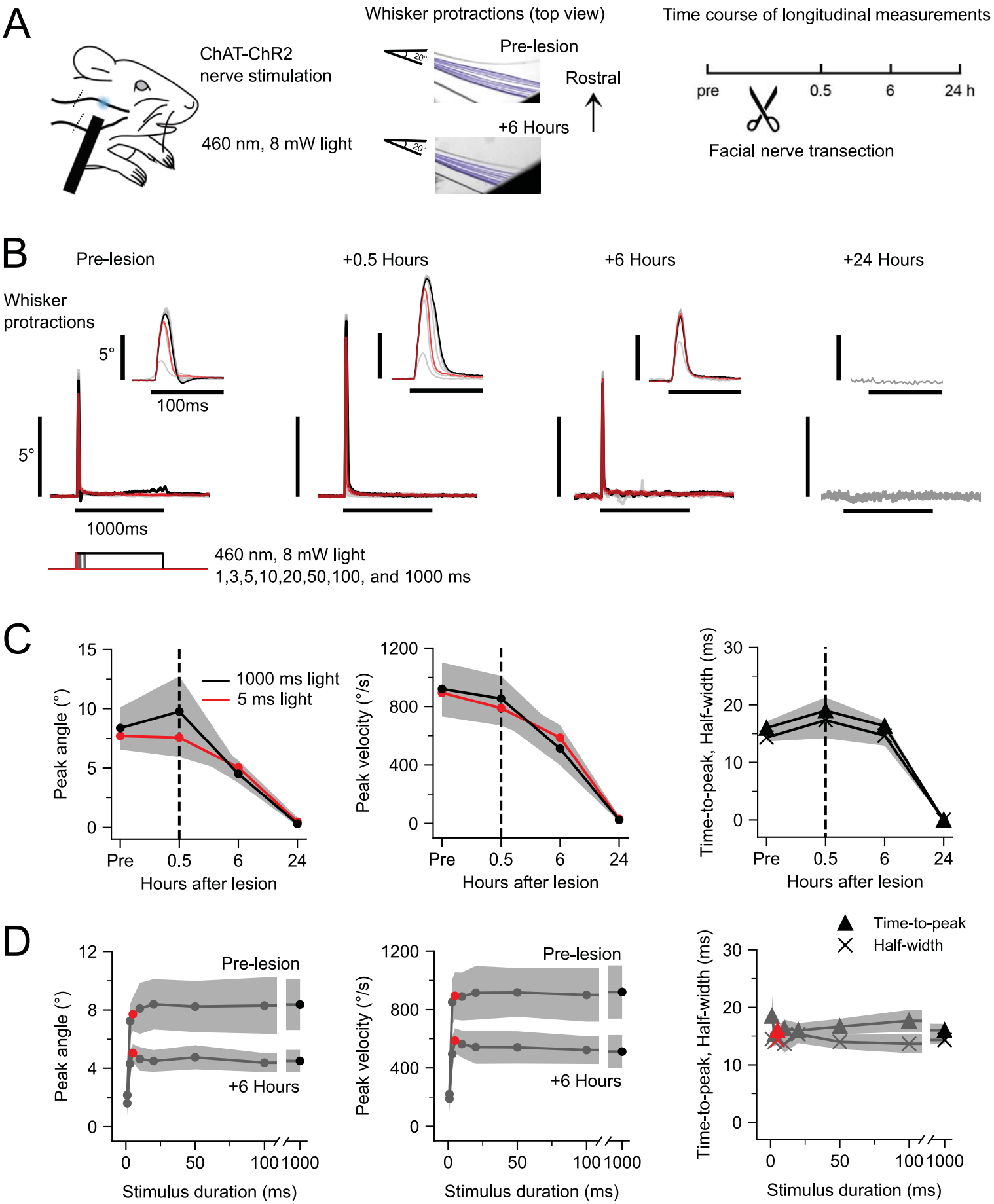
A
ChAT-ChR2
nerve stimulation
460 nm, 8 mW light
Whisker protractions (top view)
Pre-lesion
Rostral
+6 Hours
20°
Time course of longitudinal measurements
pre
0.5
6
24 h
Facial nerve transection
B
Pre-lesion
+0.5 Hours
+6 Hours
+24 Hours
Whisker
protractions
5°
100ms
5°
1000ms
460 nm, 8 mW light
1,3,5,10,20,50,100, and 1000 ms
C
1000 ms light
5 ms light
Peak angle (°)
Peak velocity (°/s)
Time-to-peak, Half-width (ms)
Pre
0.5
6
24
Hours after lesion
D
Pre-lesion
+6 Hours
Time-to-peak
Half-width
Stimulus duration (ms)

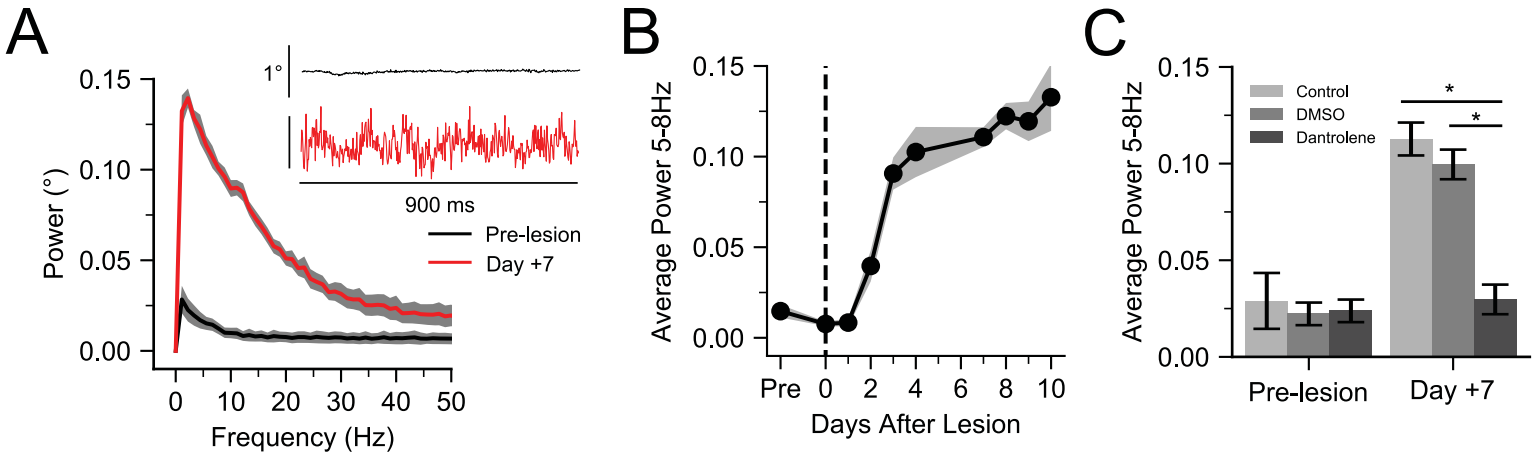
A
0.15
0.10
0.05
0.00
Power (°)
0
10
20
30
40
50
Frequency (Hz)
1°
900 ms
Pre-lesion
Day +7
B
0.15
0.10
0.05
0.00
Average Power 5-8Hz
Pre
0
2
4
6
8
10
Days After Lesion
C
0.15
0.10
0.05
0.00
Average Power 5-8Hz
Control
DMSO
Dantrolene
*
*
Pre-lesion
Day +7

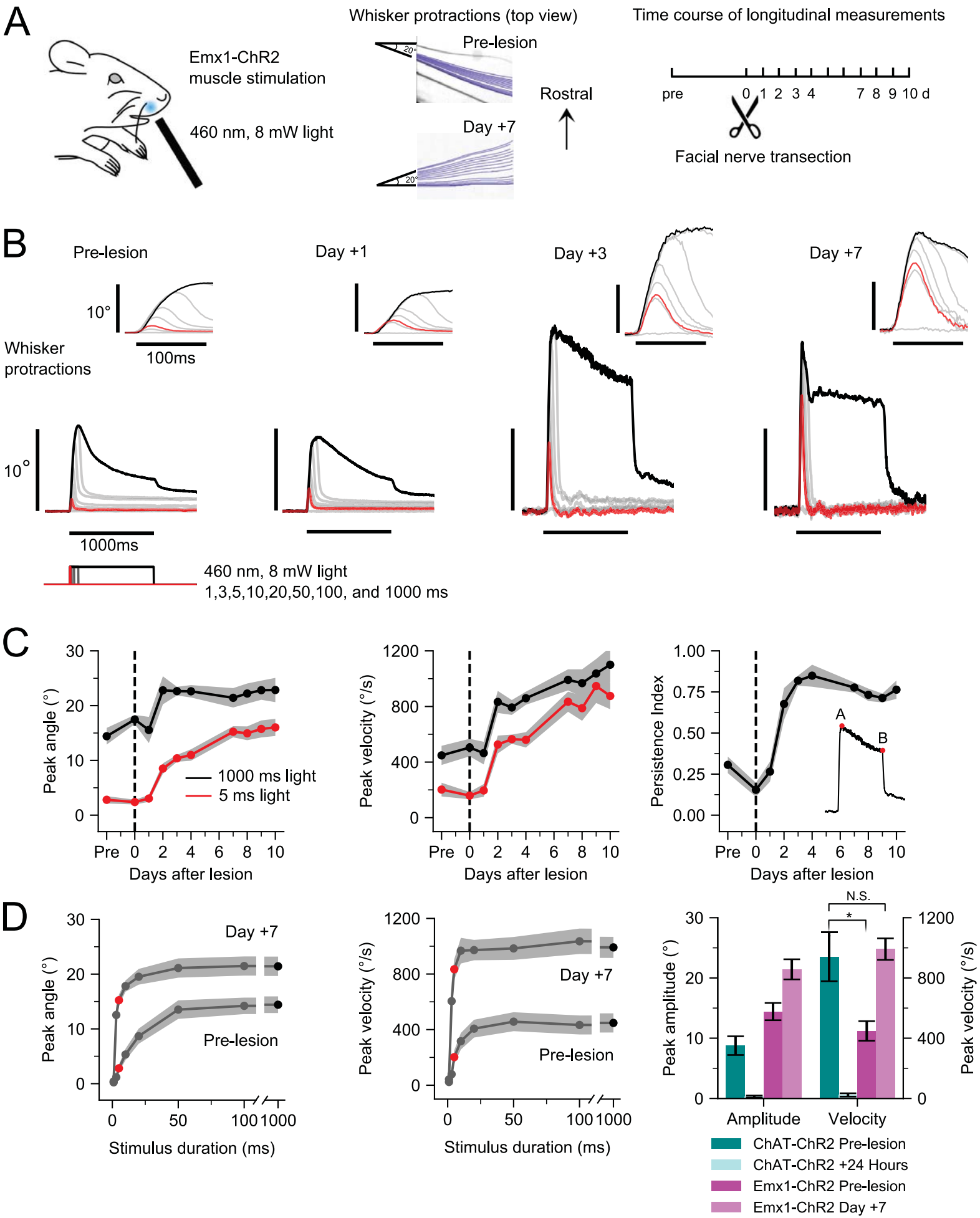
A
Emx1-ChR2
muscle stimulation
460 nm, 8 mW light
Whisker protractions (top view)
Pre-lesion
Day +7
20°
Rostral
Time course of longitudinal measurements
pre
0 1 2 3 4
7 8 9 10 d
Facial nerve transection
B
Pre-lesion
Day +1
Day +3
Day +7
10°
Whisker
protractions
100ms
10°
1000ms
460 nm, 8 mW light
1,3,5,10,20,50,100, and 1000 ms
C
Peak angle (°)
1000 ms light
5 ms light
Days after lesion
Peak velocity (°/s)
Persistence Index
A
B
D
Day +7
Pre-lesion
Stimulus duration (ms)
N.S.
*
Peak amplitude (°)
Amplitude
Velocity
ChAT-ChR2 Pre-lesion
ChAT-ChR2 +24 Hours
Emx1-ChR2 Pre-lesion
Emx1-ChR2 Day +7

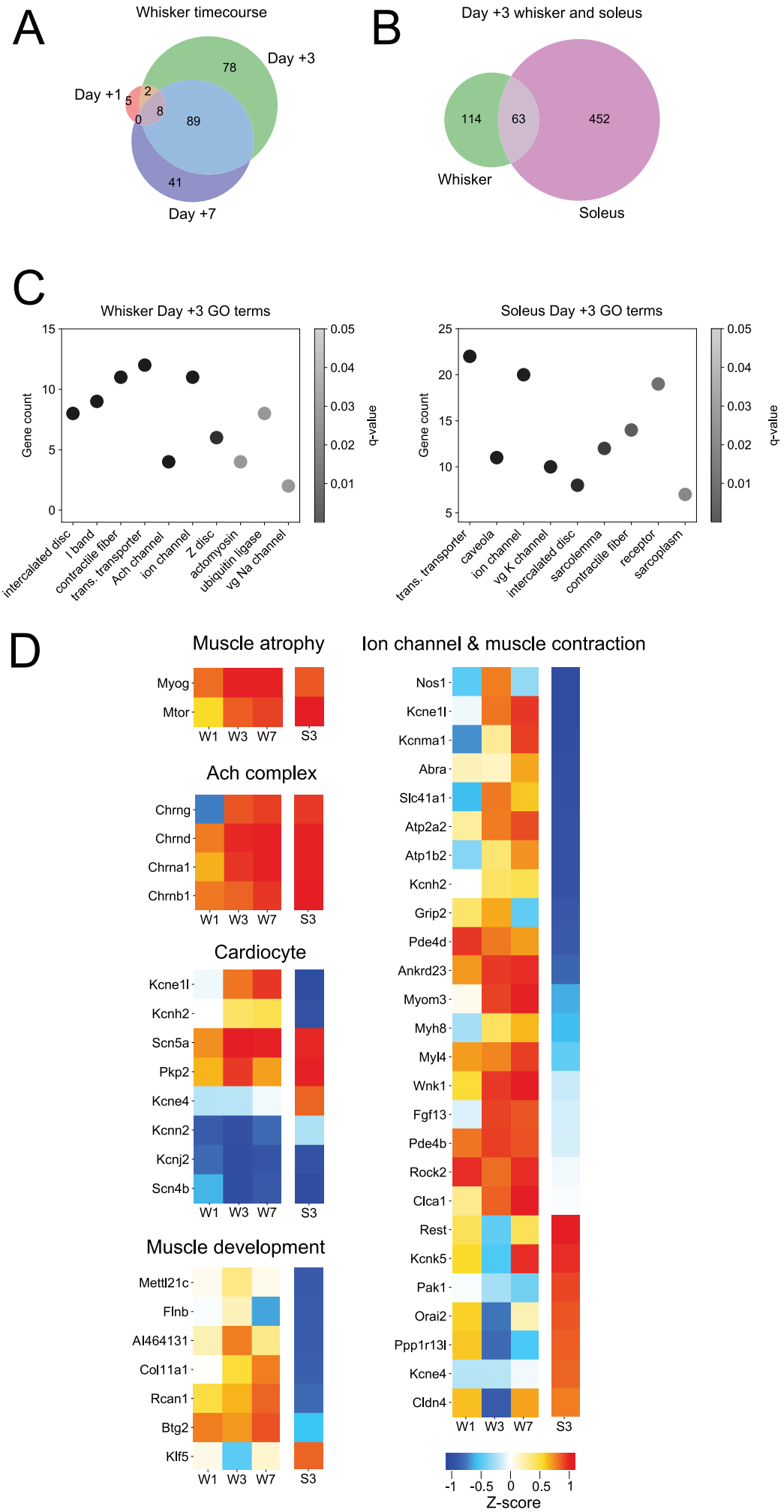
A
Whisker timecourse
Day +3
Day +1
Day +7
78
2
5
8
0
89
41
B
Day +3 whisker and soleus
114
63
452
Whisker
Soleus
C
Whisker Day +3 GO terms
Gene count
q-value
intercalated disc
I band
contractile fiber
trans. transporter
Ach channel
ion channel
Z disc
actomyosin
ubiquitin ligase
vg Na channel
Soleus Day +3 GO terms
trans. transporter
caveola
ion channel
vg K channel
intercalated disc
sarcolemma
contractile fiber
receptor
sarcoplasm
D
Muscle atrophy
Myog
Mtor
W1 W3 W7 S3
Ach complex
Chrng
Chrnd
Chrna1
Chrnb1
Cardiocyte
Kcne1l
Kcnh2
Scn5a
Pkp2
Kcne4
Kcnn2
Kcnj2
Scn4b
Muscle development
Mettl21c
Flnb
AI464131
Col11a1
Rcan1
Btg2
Klf5
Ion channel & muscle contraction
Nos1
Kcne1l
Kcnma1
Abra
Slc41a1
Atp2a2
Atp1b2
Kcnh2
Grip2
Pde4d
Ankrd23
Myom3
Myh8
Myl4
Wnk1
Fgf13
Pde4b
Rock2
Clca1
Rest
Kcnk5
Pak1
Orai2
Ppp1r13l
Kcne4
Cldn4
-1 -0.5 0 0.5 1
Z-score